Granular Matter 2, 143–152 © Springer-Verlag 2000

A macroscopic description of the quasi-static behavior of granular materials based on the theory of porous media

Stefan Diebels

Abstract Granular materials fall into the class of porous media. But in contrast to materials like foams and sponges their structure is discontinous on a microscopic level. For this reason the particles may undergo independent displacements and rotations. This is the classical kinematics which may be captured by a micropolar or *Cosserat* theory on the macroscopic level.

The goal of this paper is to combine the theory of porous media as a macroscopic theory dealing with multiphase systems and the micropolar theory describing extended kinematics and taking care of the discountinous structure of granular media on the micro scale. The resulting micropolar theory of porous media may be used to describe the quasistatic behavior of granular materials. In the present contribution thermodynamically consistent constitutive relations for the elastic response of a dense granular matrix material saturated by a viscous pore fluid are given and applied to some boundary value problems which demonstrate the physical relevance of the proposed model.

1 Introduction

Mechanical systems consisting of different components may be described on a macroscopic level using the mixture theory which was formulated in the framework of rational mechanics by Truesdell [1] and by Truesdell & Toupin [2]. Bowen introduced the volume fractions as internal variables into the mixture theory and extended it towards the theory of porous media [3,4]. Further developments of the theory of porous media (TPM) were given e.g. by de Boer & Ehlers [5] and Ehlers [6,7]. In the formulation discussed in the mentioned papers, the theory may be used to describe the behavior of porous materials such as foams on a macro scale which is much larger than the representative diameter of the pores. If one wants to model the macroscopic behavior of granular media the composition is discontinous on a micro scale. Therefore, the particles may undergo independent displacements and rotations. A macroscopic theory which is capable to deal with such a kind of extended kinematics is the micropolar or Cosserat theory [8,9], which was successfully applied to block structures [10]. Zastrau [11] stated that a micropolar approach allows to deal with the usual tools of differential calculus even for a discontinous composition on the micro scale. In addition to the physically motivated applications of the *Cosserat* theory, it was found during the last years that extended continuum theories with internal length scales lead to a regularization of the ill posed problem of softening [12].

It is the goal of this contribution to combine the theory of porous media and the micropolar theory and to develop a thermodynamically consistent model. The resulting micropolar theory of porous media (MTPM) is then able to predict the average translation and the average rotation of the granules in a representative elementary volume (REV).

In the following section the concepts of superimposed continua and of volume fractions are introduced. The extended kinematic relations of a Cosserat continuum are discussed. For a binary mixture consisting of a micropolar solid skeleton saturated by a viscous pore fluid the required balance equations are given. Starting from general results of the principle of dissipation a constitutive model is developed which describes the elastic behavior of the solid part. The plastic behavior of a micropolar solid skeleton is discussed at small strains e.g. by Ehlers & Volk [13] but for simplicity it is not included here. It is rather the goal to derive the underlying structure of such a kind of theory.

2 Kinematics

The theory of porous media is based on the idea of superimposed continua. Following this concept, it is assumed that each spatial point $\mathbf{x}$ in the current configuration is occupied by several material points of different constituents φ^α (here: skeleton $\alpha = S$, fluid $\alpha = F$). The microscopic structure of the porous medium under consideration is taken into account via the volume fractions defined as the local ratio of the volume $\mathrm{d}v^\alpha$ occupied by the constituent φ^α to the volume $\mathrm{d}v$ occupied by the whole mixture φ

$$n^\alpha = \frac{\mathrm{d}v^\alpha}{\mathrm{d}v}, \quad \alpha = S, F \ . \tag{1}$$

If the mixture is saturated, the whole space is filled with matter, i.e. taking into account that the volume of the mixture φ is given by the sum of the partial volumes of

Received: 9 June 1999

S. Diebels
Institute of Applied Mechanics (Civil Engineering)
University of Stuttgart, Pfaffenwaldring 7
D-70550 Stuttgart, Germany

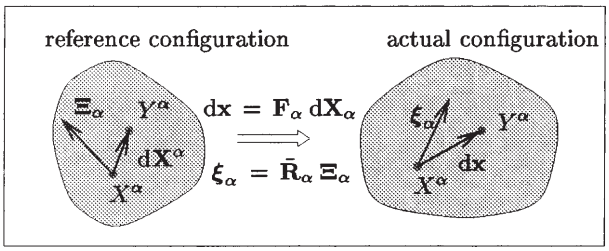

Fig. 1. Deformation gradient and micromotion

the constituents, the saturation condition is obtained in the following form

$$n^S + n^F = 1 \ . \tag{2}$$

In the same manner two different density functions may be introduced, namely the partial or bulk density ρ^α relating the element of mass $\mathrm{d}m^\alpha$ of the constituent φ^α to the volume of the whole mixture φ and the effective density $\rho^{\alpha R}$ relating the same element of mass to the volume occupied by φ^α only:

$$\rho^\alpha = \frac{\mathrm{d}m^\alpha}{\mathrm{d}v}, \quad \rho^{\alpha R} = \frac{\mathrm{d}m^\alpha}{\mathrm{d}v^\alpha}, \quad \rho^\alpha = n^\alpha \rho^{\alpha R} \ . \tag{3}$$

In this context incompressibility of one of the constituents is understood in a microscopic sense, i.e. the effective density is assumed to be constant for incompressible constituents, $\rho^{\alpha R} = \text{const}$. Even in this case the partial density may vary due to variations of the volume fraction.

Following the concept of superimposed continua, each constituent follows its own function of motion χ_α and each spatial point $\mathbf{x}$ in the current configuration is occupied by material points of each constituent, which are identified by their positions in the reference configuration $\mathbf{X}_\alpha$:

$$\mathbf{x} = \chi_\alpha(\mathbf{X}_\alpha, t) \ . \tag{4}$$

The deformation gradient

$$\mathbf{F}_\alpha = \frac{\partial \chi_\alpha(\mathbf{X}_\alpha, t)}{\partial \mathbf{X}_\alpha} \tag{5}$$

transforms line elements $\mathrm{d}\mathbf{X}_\alpha$ of the reference configuration into line elements $\mathrm{d}\mathbf{x}$ of the actual configuration (c.f. Fig. 1) so that

$$\mathrm{d}\mathbf{x} = \mathbf{F}_\alpha \, \mathrm{d}\mathbf{X}_\alpha \ . \tag{6}$$

The velocity field $\mathbf{x}'_\alpha$ is obtained from the function of motion by the time derivative

$$\mathbf{x}'_\alpha = \frac{\partial \chi_\alpha(\mathbf{X}_\alpha, t)}{\partial t} \ . \tag{7}$$

Differentiating (6) with respect to time yields

$$\mathrm{d}\mathbf{x}'_\alpha = (\mathbf{F}_\alpha)'_\alpha \, \mathbf{F}_\alpha^{-1} \, \mathrm{d}\mathbf{x} = \mathbf{L}_\alpha \, \mathrm{d}\mathbf{x} \tag{8}$$

where the spatial velocity gradient is introduced as

$$\mathbf{L}_\alpha = \operatorname{grad} \mathbf{x}'_\alpha \ . \tag{9}$$

The symbol $(\cdot)'_\alpha$ denotes the material time derivative following the motion of the constituent φ^α.

If the solid phase is assumed to be micropolar, its particles may undergo independent rotations. In this case the material points of φ^S as the carrier of the physical properties are assumed to be rigid bodies on the microscale. The independent rotational field is governed by the micromotion $\bar{\mathbf{R}}_S(\mathbf{X}_S, t)$, which is an orthogonal tensor. In order to visualise the rotation, each particle has attached a triade of rigid directors $\boldsymbol{\Xi}_S$ of fixed length, which is transformed from the reference configuration into the actual configuration according to the micromotion (c.f. Fig. 1):

$$\boldsymbol{\xi}_S = \bar{\mathbf{R}}_S \, \boldsymbol{\Xi}_S \ . \tag{10}$$

While the deformation tensors of the standard formulation of continuum mechanics are derived from squares of line elements $\mathrm{d}\mathbf{x} \cdot \mathrm{d}\mathbf{x}$, the deformation tensors of the micropolar constituent are obtained from the scalar product $\boldsymbol{\xi}_S \cdot \mathrm{d}\mathbf{x}$ of directors and line elements in the actual configuration with respect to the reference configuration or vice versa, c.f. [9,14,15]. Following this concept, the Cosserat deformation tensor of the reference configuration is given by

$$\boldsymbol{\xi}_S \cdot \mathrm{d}\mathbf{x} = \boldsymbol{\Xi}_S \cdot \bar{\mathbf{R}}_S^T \, \mathbf{F}_S \, \mathrm{d}\mathbf{X}_S \ \rightarrow \ \bar{\mathbf{U}}_S = \bar{\mathbf{R}}_S^T \, \mathbf{F}_S \ , \tag{11}$$

while the corresponding tensor of the actual configuration is given by

$$\boldsymbol{\Xi}_S \cdot \mathrm{d}\mathbf{X}_S = \boldsymbol{\xi}_S \cdot \bar{\mathbf{R}}_S \, \mathbf{F}_S^{-1} \, \mathrm{d}\mathbf{x} \ \rightarrow \ \bar{\mathbf{V}}_S = \mathbf{F}_S \, \bar{\mathbf{R}}_S^T \ . \tag{12}$$

In (11) and (12) the symbol $(\cdot)^T$ represents the transposed of a second order tensor. In analogy to the polar decomposition of the deformation gradient, $\mathbf{F}_S$ may be re-written as

$$\mathbf{F}_S = \bar{\mathbf{R}}_S \, \bar{\mathbf{U}}_S = \bar{\mathbf{V}}_S \, \bar{\mathbf{R}}_S \ , \tag{13}$$

where, in general, $\bar{\mathbf{U}}_S$ and $\bar{\mathbf{V}}_S$ are not symmetric.

Furthermore, curvature tensors are required. They describe the gradient of the micromotion. In a natural way they are introduced as third order tensors taking the derivative of the micromotion either with respect to the position $\mathbf{X}_\alpha$ of the reference configuration or $\mathbf{x}$ of the actual configuration [9,14,15]

$$\overset{3}{\mathbf{K}}_S = (\bar{\mathbf{R}}_S \operatorname{Grad}_S \bar{\mathbf{R}}_S^T)^{\underline{3}}, \ \overset{3}{\boldsymbol{\kappa}}_S = -(\bar{\mathbf{R}}_S \operatorname{grad} \bar{\mathbf{R}}_S^T)^{\underline{3}} \ . \tag{14}$$

The absolute tensor notation is used according to [16]. Taking into account the identity $\bar{\mathbf{R}}_S \, \bar{\mathbf{R}}_S^T = \mathbf{I}$, it can be shown that the curvature tensors defined in (14) are skew-symmetric with respect to the first and second index. Therefore, they may be contracted to second order curvature tensors by application of the permutation tensor $\overset{3}{\mathbf{E}}$

$$\bar{\mathbf{K}}_S = -\tfrac{1}{2}(\overset{3}{\mathbf{E}} \overset{3}{\mathbf{K}}_S)^{\underline{2}}, \quad \bar{\boldsymbol{\kappa}}_S = -\tfrac{1}{2}(\overset{3}{\mathbf{E}} \overset{3}{\boldsymbol{\kappa}}_S)^{\underline{2}} \ . \tag{15}$$

3
Balance equations

The balance equations of mixtures with an arbitrary number of micropolar constituents are discussed by Diebels & Ehlers [15] and by Diebels [17,18]. The basic idea to formulate the balance equations for mixtures is stated in Truesdell's metaphysical principles [19]. Here, these general results are specialized with respect to the binary mixture under study. From a general point of view the balances of each constituent possess the same structure as the balances of a single phase continuum. But in order to account for the interaction between the individual constituents additional production terms have to be introduced.

3.1
Balance of mass

The balance of mass for each constituent reads

$$(\rho^\alpha)'_\alpha \,+\, \rho^\alpha \,\mathrm{div}\, \mathbf{x}'_\alpha \,=\, \hat{\rho}^\alpha \quad . \tag{16}$$

In (16), $\mathrm{div}(\cdot)$ is the divergence corresponding to $\mathrm{grad}(\cdot) = \partial(\cdot)/\partial\,\mathbf{x}$. In general, an exchange of mass is possible between the constituents, i.e. $\hat{\rho}^\alpha \neq 0$, e.g. to model the melting of ice in an ice-water mixture. But here it is assumed that there is no phase transition between the solid and the fluid constituent. Therefore, $\hat{\rho}^\alpha = 0$. As usual in solid mechanics, equation (16) with $\alpha = S$ may be integrated from the density ρ^S_{0S} of the reference configuration to the actual value ρ^S yielding

$$\rho^S \,=\, \rho^S_{0S}\, \det \mathbf{F}_S^{-1} \quad . \tag{17}$$

The volumetric deformation $J_S = \det \mathbf{F}_S$ gives rise to a change of the effective density ρ^{SR} and of the volume fraction n^S.

3.2
Balance of linear momentum

Following Newton's axiom the change of momentum of a body is equal to the forces acting on it. With the partial stress tensor $\mathbf{T}^\alpha$ and with the body forces $\rho^\alpha\,\mathbf{b}$ the balance of linear momentum is obtained in its local form:

$$\rho^\alpha\,\mathbf{x}''_\alpha \,=\, \mathrm{div}\,\mathbf{T}^\alpha \,+\, \rho^\alpha \mathbf{b} \,+\, \hat{\mathbf{p}}^\alpha \quad . \tag{18}$$

In (18) $\hat{\mathbf{p}}^\alpha$ is the exchange of momentum or, in the context of the binary model, the interaction force per unit of bulk volume. In order to preserve the linear momentum of the mixture, the sum of the interaction forces must vanish so that

$$\hat{\mathbf{p}}^S \,=\, -\,\hat{\mathbf{p}}^F \quad . \tag{19}$$

Both, $\mathbf{T}^\alpha$ and $\hat{\mathbf{p}}^\alpha$, must be given by constitutive relations.

3.3
Balance of moment of momentum

It is well known in mechanics of non-polar materials that the balance of moment of momentum leads to symmetric *Cauchy* stress tensors. Therefore for the non-polar fluid one has

$$\mathbf{T}^F \,=\, (\mathbf{T}^F)^T \quad . \tag{20}$$

If the solid skeleton under consideration is assumed to be micropolar the material points are regarded as rigid bodies on the microscale, i.e. they possess a spin and a corresponding microinertia. For simplicity the microinertia is represented by an isotropic tensor $\Theta^S\,\mathbf{I}$ and, therefore, it is constant under the motion of the rigid micro particles. Otherwise the so-called balance of microinertia must be taken into account [15,18,20]. The local form of the balance of moment of momentum reads

$$\rho^S\,\Theta^S\,(\bar{\boldsymbol{\omega}}_S)'_S \,=\, \mathrm{div}\,\mathbf{M}^S \,+\, \mathbf{I}\times\mathbf{T}^S \,+\, \rho^S\,\mathbf{c}^S \,+\, \hat{\mathbf{m}}^S \quad . \tag{21}$$

The angular velocity $\bar{\boldsymbol{\omega}}_S$ related to the micromotion may be computed as

$$\bar{\boldsymbol{\omega}}_S \,=\, \tfrac{1}{2}\overset{3}{\mathbf{E}}\big((\bar{\mathbf{R}}_S)'_S\,\bar{\mathbf{R}}_S^T\big) \quad . \tag{22}$$

The product $\mathbf{I}\times\mathbf{T}^S$ represents twice the axial vector of the Cauchy stress $\mathbf{T}^S$. For symmetric stress tensors it is zero. $\mathbf{M}^S$ are the couple stresses. The volumetrically distributed moments $\rho^S\,\mathbf{c}^S$ (supply terms) are included during the evaluation of the entropy principle but they are neglected in the examples presented below due to the fact that no electro-magnetic forces are taken into account. In addition, the interaction $\hat{\mathbf{m}}^S$ is equal to zero because the fluid is assumed to be non-polar and, therefore, it is not able to transfer moments.

In a more general model, further balances are the balance of energy and the entropy inequality. Both balances are discussed in detail by Diebels [17,18] and by Diebels & Ehlers [15] in the framework of micropolar mixtures. In the present contribution these equations are not discussed but the relations obtained form the evaluation of the entropy inequality and the principle of dissipation are summarized in the next section. They highlight the structure which is required in a micropolar mixture theory with compressible constituents.

4
Constitutive equations

The balance equations discussed in the last section are independent of the material behavior. In order to close the set of balance equations further equations, the so-called constitutive equations, are required. They describe the behavior of the special material under study. In the present investigation the porous solid phase is assumed to be micropolar, elastic, and saturated by a viscous pore fluid. The corresponding set of variables is given by

$$\begin{aligned}\mathscr{S} = \{&\bar{\mathbf{U}}_S,\, \mathrm{Grad}_S\,\bar{\mathbf{U}}_S,\, \bar{\mathbf{K}}_S,\, \mathrm{Grad}_S\,\bar{\mathbf{K}}_S,\\ &\rho^F,\mathrm{grad}\,\rho^F,\, \mathbf{D}_F,\, \mathbf{w}_F,\, n^S,\, \mathrm{grad}\,n^S,\, \vartheta,\, \mathrm{grad}\,\vartheta\} \quad .\end{aligned} \tag{23}$$

Therein,

$$\mathbf{D}_F \,=\, \tfrac{1}{2}\big(\mathbf{L}_F \,+\, \mathbf{L}_F^T\big) \tag{24}$$

is the stretching tensor, i.e. the symmetric part of the velocity gradient,

$$\mathbf{w}_F \,=\, \mathbf{x}'_F \,-\, \mathbf{x}'_S \tag{25}$$

is the seepage velocity, and ϑ is the absolute temperature, which is assumed to be the same for both constituents. The set of response functions

$$\mathscr{R} = \{\eta^\alpha, \boldsymbol{\phi}_\eta^\alpha, \psi^\alpha, \mathbf{T}^\alpha, \mathbf{M}^S, \hat{\mathbf{p}}^F, (n^S)'_S\} \tag{26}$$

must be given by the constitutive equations. Therein, η^α is the entropy, $\boldsymbol{\phi}_\eta^\alpha$ is the entropy flux, and ψ^α is the free energy function of the constituent φ^α. As an *a priori* constitutive equation the entropy flux $\boldsymbol{\phi}_\eta^\alpha$ is given in terms of the heat flux $\mathbf{q}^\alpha$ and the temperature ϑ

$$\boldsymbol{\phi}_\eta^\alpha = \frac{\mathbf{q}^\alpha}{\vartheta} \ . \tag{27}$$

More general relations for $\boldsymbol{\phi}_\eta^\alpha$ are possible within the framework of the Liu-Müller evaluation of the entropy principle [21,22], probably the couple stresses and the momentum supply, respectively, will enter into (27). In the present article the more restrictive evaluation of the entropy principle formulated as *Clausius-Duhem* inequality is applied according to Coleman & Noll [23].

4.1
Evolution of the volume fraction

Due to the fact that the volume fractions are introduced as internal variables, there are no balance equations for them. As usual for internal variables evolution equations must be formulated in the framework of the constitutive theory. In the present contribution, an evolution equation for the solid matrix is motivated from the balance of mass. Changes of the partial density ρ^S are possible due to two different effects according to $(3)_3$: One possibility is the change of the effective density, the other one is given by changes in the volume fraction. The balance of mass for the solid phase may be re-written under this point of view in the following form

$$\begin{aligned} &\rho^{SR} \quad \left[(n^S)'_S + z^S\, n^S \operatorname{div} \mathbf{x}'_S\right] \\ &+ n^S \left[(\rho^{SR})'_S + (1 - z^S)\, \rho^{SR} \operatorname{div} \mathbf{x}'_S\right] = 0 \ . \end{aligned} \tag{28}$$

In this equation the function $0 \leq z^S \leq 1$ determines the percentage of the change of density which is governed by changes of the volume fraction n^S. Assuming that ρ^{SR} and n^S are independent variables in the process under study, each bracket in equation (28) must vanish seperately. From this assumption the required evolution equation is obtained constitutively in the following form

$$(n^S)'_S + z^S\, n^S \operatorname{div} \mathbf{x}'_S = 0 \ . \tag{29}$$

For $z^S = 1$, (29) degenerates to the volume balance known from incompressible porous materials [3,24,25]. In order to model reversible behavior of the elastic skeleton, (29) may be integrated yielding an equation of state. This does not introduce dissipation into the model. For plastic behavior of the skeleton dissipative mechanisms may easily be incorporated into (29).

In addition, the evolution of the volume fraction n^F is governed by the saturation constraint. From the microscopic point of view this is valid for a gas which always fills the pore space. Taking the material time derivative of the saturation condition (2) following the motion of the skeleton and transforming $(n^F)'_S$ into $(n^F)'_F$ by

$$(n^F)'_S = (n^F)'_F - \operatorname{grad} n^F \cdot \mathbf{w}_F \tag{30}$$

yields the required equation in the form

$$(n^F)'_F = z^S\, n^S \operatorname{div} \mathbf{x}'_S - \operatorname{grad} n^S \cdot \mathbf{w}_F \ . \tag{31}$$

Taking into account (29) and (31), a saturation pressure does not explicitly arise in the theory if the fluid is compressible.

4.2
Results from the entropy principle

The following results are sufficient to satisfy the principle of dissipation for a *Cosserat*-elastic compressible matrix saturated by a viscous compressible pore-fluid under isothermal conditions. For details, c.f. [18]. Even more general results are obtained by Svendsen & Hutter [25] for non-polar mixtures including constraints like incompressibility. For simplicity, isothermal conditions and the principle of phase seperation [24] are assumed:

– The stress tensor in the solid matrix is governed by two parts, namely

$$\mathbf{T}^S = \bar{\mathbf{R}}^S \left[\rho^S \frac{\partial \psi^S}{\partial \bar{\mathbf{U}}_S}\right] \mathbf{F}_S^T - z^S n^S \left[p^{FR} + p^K\right] \mathbf{I} \ . \tag{32}$$

Therein, the first term on the right hand side is the so-called extra stress

$$\mathbf{T}_E^S = \bar{\mathbf{R}}^S \left[\rho^S \frac{\partial \psi^S}{\partial \bar{\mathbf{U}}_S}\right] \mathbf{F}_S^T \tag{33}$$

resulting from the macroscopic deformation of the matrix material. The second term depends on the effective fluid pressure

$$p^{FR} = \left(\rho^{FR}\right)^2 \frac{\partial \psi^F}{\partial \rho^{FR}} \tag{34}$$

and on the so-called configuration pressure

$$p^K = \rho^F \frac{\partial \psi^F}{\partial n^S} + \rho^S \frac{\partial \psi^S}{\partial n^S} \tag{35}$$

resulting from changes in porosity. Furthermore, the free energy functions ψ^α serve as potentials for the extra stress and for the fluid pressure.

– The couple stresses of the solid matrix follow from the free energy function ψ^S by differentiation with respect to the curvature tensor

$$\mathbf{M}^S = \bar{\mathbf{R}}_S \left[\rho^S \frac{\partial \psi^S}{\partial \bar{\mathbf{K}}_S}\right] \mathbf{F}_S^T \ . \tag{36}$$

– The fluid stresses depend on the effective fluid pressure p^{FR} and on an extra term governed by a positive definite material tensor $\overset{4}{\mathbf{T}}$ and the stretching $\mathbf{D}_F$:

$$\mathbf{T}^F = -\, n^F p^{FR} \mathbf{I} + \mathbf{T}_E^F = -\, n^F p^{FR} \mathbf{I} + \overset{4}{\mathbf{T}}\, \mathbf{D}_F \ . \tag{37}$$

As usual in hydraulics and ground water flow the fluid extra stresses $\mathbf{T}_E^F$ are neglected with respect to the interaction force:

$$\mathbf{T}_E^F = \overset{4}{\mathbf{T}}\,\mathbf{D}_F \approx \mathbf{0} \ . \tag{38}$$

A validation of this common assumption in terms of non-dimensional characteristic numbers is given in [26].
Like the stresses, the exchange of momentum or the interaction force per unit of bulk volume is split into two parts, one of them depending on the gradient of the volume fraction and the other one, the so-called extra term, depending on the seepage velocity $\mathbf{w}_F$

$$\hat{\mathbf{p}}^F = -\left[p^{FR} + \rho^F \frac{\partial \psi^F}{\partial n^S}\right] \operatorname{grad} n^S - \mathbf{P}\,\mathbf{w}_F \ . \tag{39}$$

According to [27,28] the first term of the r.h.s. of (39) is called interaction of *Fick*ian type and the second of *Darcy* type. Therein, it is shown that $\partial\psi^F/\partial n^S$ becomes important in some applications, but here it is assumed that $\psi^F = \psi^F(\rho^{FR})$, which leads to reasonable results in several applications.
The tensor $\mathbf{P}$ is symmetric and positive definite. In the case of an isotropic pore structure the tensor $\mathbf{P}$ becomes spherical:

$$\mathbf{P} = \frac{(n^F)^2\,\gamma^{FR}}{k^F}\,\mathbf{I} \ , \tag{40}$$

where γ^{FR} is the effective weight of the fluid and k^F is the so-called *Darcy* permeability containing information on the size and structure of the pore space and on the viscosity of the fluid. Inserting (38) and (40) into the quasi-static form of the balance of momentum of the fluid (equation (18) with $\alpha = F$ and $\rho^F\,\mathbf{x}_F'' \approx \mathbf{0}$), the well-known *Darcy* law is recovered if ψ^F does not depend on the volume fraction n^S:

$$n^F\,\mathbf{w}_F = \frac{k^F}{\gamma^{FR}}\left(\rho^{FR}\,\mathbf{b} - \operatorname{grad} p^{FR}\right) \ . \tag{41}$$

The presented relations obtained from the principle of dissipation may directly be extended to more general conditions including thermal effects and further couple terms due to the principle of equipresence [18]. On the other hand, to become more specific, the free energy functions ψ^α must be specialized.

4.3 Free energy functions

For the sake of simplicity the fluid is assumed to be an ideal gas. Consequently, under isothermal conditions the pressure is directly related to the effective density. More general equations of state are discussed and applied in [26]. With a constant factor κ^F the constitutive relation applied in the examples reads

$$p^{FR} = \kappa^F\,\rho^{FR} \ . \tag{42}$$

The free energy function ψ^F may be obtained by integration of (42)

$$\psi^F = \kappa^F \ln(\rho^{FR}/\rho_0^{FR}) + \psi_0^F \ . \tag{43}$$

In (43) ρ_0^{FR} and ψ_0^F are the values of the effective density and of the free energy at a given reference pressure p_0^{FR}, respectively.

For the solid the situation is more complicated. In the case of isotropic behavior the free energy may be given as an isotropic function of the invariants of the deformation tensor and of the curvature tensor [29]. The following form is chosen:

$$\begin{aligned}\rho_{0S}^S\,\psi^S = {}& \mu^S(\mathrm{II}_U - \ln J_S - 3/2) + \mu_c^S(\mathrm{II}_U - \mathrm{IV}_U) \\ & + \lambda^S\left[\beta\,W^S(J_S) + (1-\beta)W^S(n_{0S}^S/n^S)\right] \\ & + \mu_c^S\,(l_c^S)^2\,f(J_S)\,\mathrm{II}_K + P_0\,J_S \ .\end{aligned} \tag{44}$$

The invariants used in (44) are:

$$\begin{aligned}\mathrm{II}_U &= \tfrac{1}{2}\bar{\mathbf{U}}_S \cdot \bar{\mathbf{U}}_S, \\ \mathrm{IV}_U &= \tfrac{1}{2}\bar{\mathbf{U}}_S \cdot \bar{\mathbf{U}}_S^T, \\ J_S &= \det \bar{\mathbf{U}}_S = \det \mathbf{F}_S = J_S, \\ \mathrm{II}_K &= \tfrac{1}{2}\bar{\mathbf{K}}_S \cdot \bar{\mathbf{K}}_S \ .\end{aligned} \tag{45}$$

The material parameters arising in (44) are the classical *Lamé* constants λ^S and μ^S. In addition, μ_c^S is a *Cosserat* parameter and l_c^S is the so-called internal length. The parameter β takes care of the two different compressibilities, one of them related to macroscopic deformations in terms of J_S, the other one in terms of changes in the volume fraction n_{0S}^S/n^S. The initial pressure P_0 is neccessary to ensure equilibrium in the reference configuration where the fluid constituent is under the pressure p_0^{FR} while the skeleton is undeformed. As discussed in [30] the volumetric part of the free energy function may be given by

$$W^S(x) = \frac{1}{4}\left[(x-1)^2 + (\ln x)^2\right] \ . \tag{46}$$

This guarantees that the physical limits for the free energy function and for the stresses under infinite extension and compression are met: Infinite deformations require the free energy and the stresses to become infinite, too.

Finally, the function $f(J_S)$ allows for an increase of the couple stresses with increasing compression if f is chosen as

$$f(J_S) = J_s^{-m}, \quad m \geq 0 \ . \tag{47}$$

From (44) the weighted *Cauchy* extra stresses, the configuration pressure, and the weighted couple stresses may be computed according to equations (32), (35), and (36), respectively:

– Weighted *Cauchy* extra stresses:

$$\begin{aligned}J_S\,\mathbf{T}_E^S = {}& \mu^S\,(\mathbf{B}_S - \mathbf{I}) + \mu_c^S\,(\mathbf{B}_S - (\bar{\mathbf{V}}_S^T)^2) \\ & + \lambda^S\,\beta\,J_S\,\frac{\mathrm{d}W^S(J_S)}{\mathrm{d}J_S}\,\mathbf{I} \\ & + \mu_c^S\,(l_c^S)^2\,J_S\,\frac{\mathrm{d}f(J_S)}{\mathrm{d}J_S}\,\mathrm{II}_K\,\mathbf{I} + J_S\,P_0\,\mathbf{I}\end{aligned} \tag{48}$$

with the symmetric left *Cauchy-Green* deformation tensor

$$\mathbf{B}_S = \mathbf{F}_S\,\mathbf{F}_S^T = \bar{\mathbf{V}}_S\,\bar{\mathbf{V}}_S^T \ . \tag{49}$$

– Configuration pressure:

$$p^K = -\frac{(1-\beta)\,\lambda^S\, n_{0S}^S}{2\,J^S\,(n^S)^2} \left(\frac{n_{0S}^S}{n^S} - 1 + \frac{n^S}{n_{0S}^S}\,\ln\frac{n_{0S}^S}{n^S}\right) . \tag{50}$$

– Weighted couple stresses:

$$J_S\,\mathbf{M}^S = \mu_c^S\,(l_c^S)^2\,f(J_S)\,\boldsymbol{\kappa}_S\,\mathbf{B}_S . \tag{51}$$

If the micromotion $\bar{\mathbf{R}}_S$ is identical with the continuum rotation $\mathbf{R}_S$ following from the polar decomposition of the deformation gradient,

$$\mathbf{F}_S = \mathbf{R}_S\,\mathbf{U}_S = \mathbf{V}_S\,\mathbf{R}_S , \tag{52}$$

the second term on the r.h.s. of equation (48) vanishes and the stress tensor becomes symmetric. The terms in equation (48) related to the classical *Lamé* constants represent a volumetrically extended Neo-*Hooke* law. Furthermore, for the choice $m = 0$ the couple stress tensor is given in the well-known form proposed by de Borst [31] in the linear case and extended into the range of finite deformations by Steinmann [14]. In equation (51) the left *Cauchy-Green* deformation tensor $\mathbf{B}_S$ appears only due to geometrical non-linearities.

4.4
The principle of effective stress

Taking into account the principle of effective stress in the form given by Šuklje [32], the factor z^S resulting form the evolution equation (29) may be determined. According to that principle, the total hydrostatic stress σ is governed on the one hand by the fluid pressure p^{FR} and on the other hand by the effective stress σ'. The latter one is the part of the stress derived from the free energy function of the solid skeleton by differentiation with respect to the deformation. Šuklje stated the principle of effective stress in the following form:

$$\sigma = \sigma' + \left(1 - n^S\,\frac{K^S}{K^{SR}}\right) p^{FR} . \tag{53}$$

Therein, K^S is the compressibility of the porous skeleton and K^{SR} is the compressibility of the matrix material itself. This result must be compared with the negative spherical part of the total stress resulting from (32) and (37), i.e. with

$$\sigma = -\tfrac{1}{3}(\mathbf{T}^F + \mathbf{T}^S)\cdot\mathbf{I} . \tag{54}$$

Identifying the effective stress with the parts of $\mathbf{T}^S$ which are related to the free energy ψ^S leads to a function z^S that is governed by the ratio of the moduli K^S and K^{SR}, respectively:

$$z^S = 1 - \frac{K^S}{K^{SR}} . \tag{55}$$

If the matrix material is incompressible $K^{SR} \to \infty$, and, as a consequence, $z^S \to 1$ which transforms the evolution equation (29) into the well-known balance of volume valid for incompressible constituents. Furthermore, it is assumed that K^S is proportional to K^{SR} by the volume fraction n^S. This corresponds to the so-called Voigt bound of homogenization theory. In this case, the function z^S is obtained in the simple form

$$z^S = 1 - n^S = n^F \tag{56}$$

and the evolution equation (29) may be integrated yielding

$$n^S = \frac{n_{0S}^S}{n_{0S}^S(1 - J_S) + J_S} . \tag{57}$$

4.5
The hybrid and the incompressible model

In many cases, the structural compressibility of the skelton material is much larger than the compressibility of the grains themselves. Therefore, the effective density of the solid phase is assumed to be constant, ρ^{SR} =const., and the balance of mass degenerates to a balance of volume. This requires that the function $z^S = 1$. Integration of (29) directly yields the well-known result

$$n^S = n_{0S}^S\,J_S^{-1} . \tag{58}$$

The volume fractions are no longer independent process variables, but they may be expressed by J_S according to (58). Instead of (32) the stresses are given by the relation

$$\mathbf{T}^S = \bar{\mathbf{R}}^S\left[\rho^S\,\frac{\partial\psi^S}{\partial\bar{\mathbf{U}}_S}\right]\mathbf{F}_S^T - n^S\,p^{FR}\,\mathbf{I} . \tag{59}$$

Furthermore, while (44) remains unchanged, the volumetric part of the free energy function must by modified in order to take care of the point of compaction: If all pores are closed, further compression is not possible. Ehlers & Eipper modelled the point of compaction by the following volumetric part of the free energy function [33]:

$$W^S(J_S) = (1 - n_{0S}^S)^2\left[\frac{J_S - 1}{1 - n_{0S}^S} - \ln\left(\frac{J_S - n_{0S}^S}{1 - n_{0S}^S}\right)\right] . \tag{60}$$

The model consisting of an incompressible solid skeleton saturated by a compressible pore-fluid is called the hybrid model (of second type) [7,17,18,34].

The so-called incompressible model is obtained if both, the solid and the fluid, are assumed to be incompressible. In addition to the modifications (58)–(60), the pore pressure is no longer given by an equation of state but it degenerates to a Lagrangean multiplier to guarantee the saturation constraint, i.e. in this case the saturation pressure enters the model explicitly.

5
Examples

The micropolar two-phase model discussed in the previous sections was implemented into the finite element code PANDAS [35], which was developed at the Institute of Applied Mechanics (Civil Engineering) at the University

of Stuttgart. Details of the weak formulation of the balance equations and of the numerical implementation may be found in [36–38].

In this section some representative elementary experiments are computed in order to validate the model and to show its physical relevance. The presented examples are based on the quasi-static formulation of the balance equations. Furthermore, plain strain is assumed in the two-dimensional examples. The parameters listed in Table 1 were used during the computations if nothing else is specified in the examples.

5.1 Uniaxial tension test

The uniaxial tension test is the simplest test that may be simulated. It may be performed under drained or undrained conditions. In the first case only the properties of the solid phase are of interest, while in the second case the properties of both constituents influence the resulting curves.

The force which is required to elongate a 0.2 m long and 0.1 m wide specimen by the given amount is shown in Fig. 2 for drained conditions and in Fig. 3 for undrained conditions. The strain under extension is 200% and under compression −90%. In the case of granular materials only the range of compression is of interest but the rage of extension may be relevant for foams and sponges.

The different curves show the results for the compressible model with $\beta = 0$ and $\beta = 1$ and for the incompressible model. The rotational degrees of freedom related to the micropolar properties of the skeleton are not activated in this example.

The major differences between the compressible and incompressible models are found in the range of compression. Under the same axial load the incompressible model leads to smaller displacements than the compressible model. This is a result of the point of compaction included into the incompressible model: If all pores are closed the incompressible model does not allow for further compression while from the theoretical point of view the compressible model may be compressed to zero volume under infinite hydrostatic stresses. In the compressible model an adjustment of the load-displacement curves in a certain range is possible by variation of the parameter β. For $\beta = 0$ only the configuration pressure p^K is active

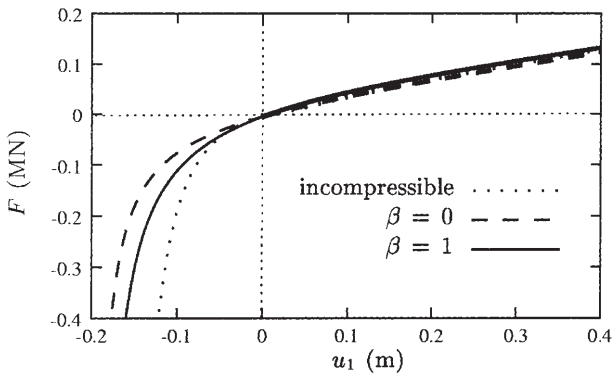

Fig. 2. Force-displacement-diagram (drained conditions)

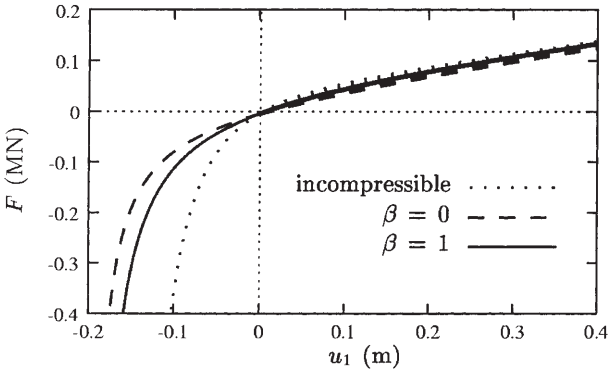

Fig. 3. Force-displacement-diagram (undrained conditions)

Table 1. Used parameters

μ^S	1.33	MN/m^2
μ_c^S	0.67	MN/m^2
λ^S	1.33	MN/m^2
l_c^S	0.01	m
m	2	
β	0, 0.5 and 1	
n_{0S}^S	0.7	
ρ_{0S}^{SR}	3000	kg/m^3
ρ_{0S}^{FR}	1000	kg/m^3 (incompressible fluid)
κ^F	0,1	MNm (compressible fluid)
k^F	$1 \cdot 10^{-4}$	m/s

and determines the hydrostatic stress in the solid skeleton while in the limit $\beta = 1$ the structural compressibility governs this stress.

Fig. 4 shows the lateral displacement over the elongation of the specimen for drained conditions. It can be seen that the local *Poisson* ratio ν^S defined as negative ratio of transversal to longitudinal strain is always positive. This physically meaningful result is not guaranteed in finite elasticity if the free energy function is split into isochoric and volumetric parts without any coupling [39]. Due to the point of compaction the largest values of the *Poisson* ratio are predicted by the incompressible model under compres-

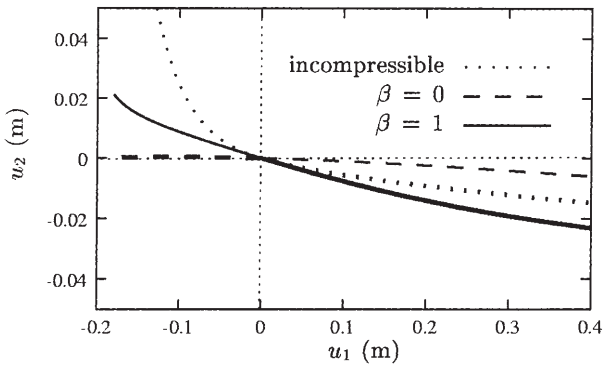

Fig. 4. Lateral displacement over elongation

sion when the pores are closed. For the undrained case the effect is even stronger because the specimen has to deform under constant total volume and no shrinkage of the pore space is possible for the incompressible pore fluid.

5.2 Consolidation test

Another one-dimensional example is the consolidation problem. A specimen of 1 m width is loaded on the top. Only the surface is drained while all other boundaries are rigid and undrained. When the load is applied the fluid starts to drain. Fig. 5 shows the vertical displacement (settlement) of the top under a load that is increased linearly in time and then kept constant at $t = 1$ s. Thereafter, the applied load is 0.1 MNm^{-2}.

While the compressible ($\beta = 0.5$) and the hybrid model show a relatively spontaneous settlement the incompressible model reacts with a strong time dependence. This is due to the fact that the incompressible model requires the pore fluid to be flown out before a settlement is possible. On the other hand, in the models with a compressible pore fluid, a volumetric deformation is possible even when the fluid still fills the pores. In contrast to the short time behavior, the long time behavior is governed by the compressibility of the skeleton, which is greater in the compressible model than in the hybrid and in the incompressible model. Therefore, under the same load, the compressible model shows a greater settlement than the models with incompressible matrix material.

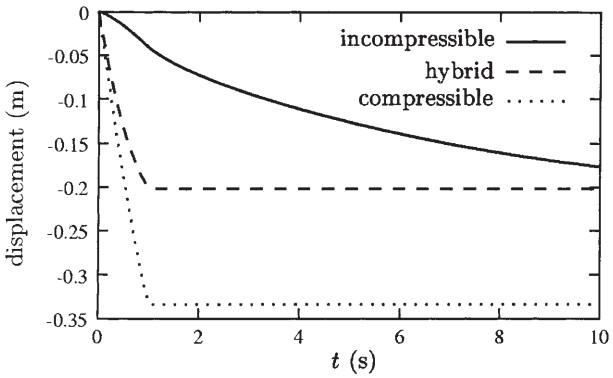

Fig. 5. Settlement under step load

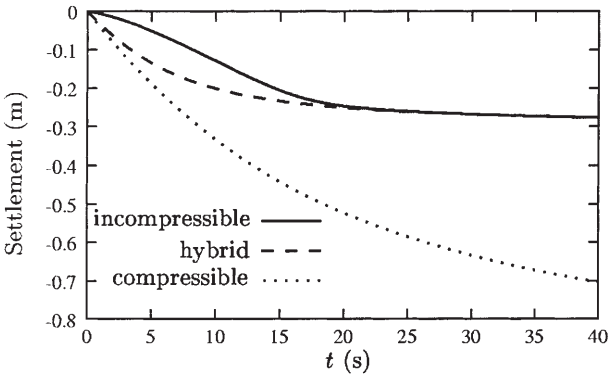

Fig. 6. Settlement under linearly increasing load

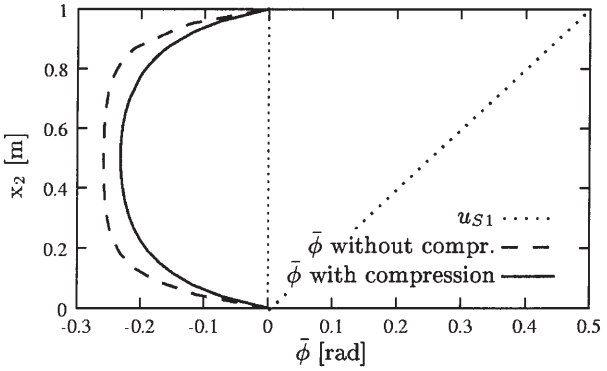

Fig. 7. Displacement and rotation under shear

If the load is continously increased with a rate of 10 $\mathrm{kNm}^{-2}\mathrm{s}^{-1}$, effects due to the point of compaction become visible in Fig. 6 for the hybrid and incompressible model, respectively. While an increase of the load leads to an increase of the surface displacement in the compressible model, the models including an incompressible skeleton do not allow a further compression if the point of compaction is reached. An increase of the load does not lead to further settlement in this case.

Both uni-axial tests, the tension test and the consolidation test, do not activate the additional degrees of freedom related to the micropolar solid phase. The material parameters related to the standard part of the model may be determined by these experiments.

5.3 Shear test

The simplest example which allows for independent rotations is the shear test. In this example a layer of 1 m thickness is sheared horizontally. Zero boundary conditions are given for the displacement and for the micropolar rotation on the lower surface, the upper surface is displaced horizontally with zero rotation. In a second experiment, an additional compression is applied to the upper surface. Therefore, the effective internal length $l_c^S \sqrt{f(J_S)}$ is increased which leads to an increase of the influence of the zero boundary conditions and a decrease of the maximum value of $\bar{\phi}$.

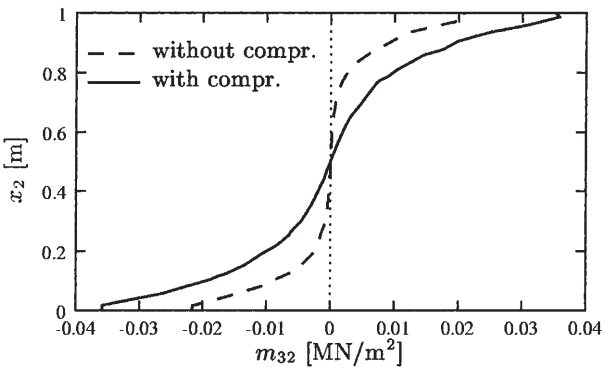

Fig. 8. Couple stresses

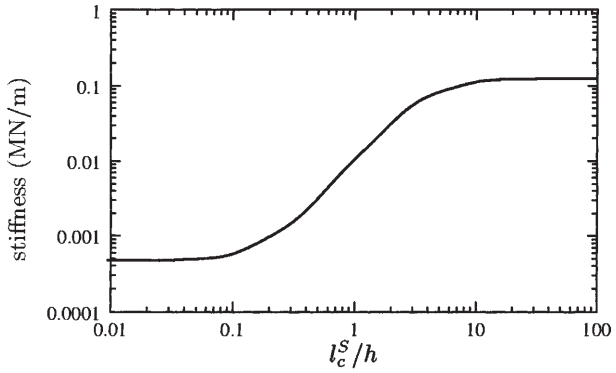

Fig. 9. Size effect under bending

As can be seen from the results in Fig. 7 the effective internal length strongly influences the distribution of the rotations, while the horizontal displacment is independent of the value of this parameter. For small internal length scales the solution shows a typical boundary layer character, the limit $l_c^S \to 0$ leads to a singular perturbed problem with constant rotation over the thickness of the specimen. In this case the boundary conditions $\bar{\phi} = 0$ can not be fullfilled at the lower and upper boundaries.

The corresponding graph of the couple stresses in Fig. 8 shows the same boundary layer structure. The thickness of the boundary layer decreases with decreasing internal length scales. In the regions with large gradients of the rotational angle, i.e. with large curvature, the couple stresses are big while in the middle of the specimen no couple stresses occur.

The boundary layer character of the rotational degree of freedom and of the couple stress allows to conclude for the additional parameters of the micropolar part of the model.

5.4 Bending test

A further example where the rotational degrees of freedom are activated is the bending test of a narrow beam. Lakes [40,41] found that under bending the *Cosserat* continuum shows a size effect which leads to a stiffness of the beam which depends on the ratio of the internal length l_c^S to the width h of the beam. This result is verified using the model presented above. Therefore, a single ended clamped beam with a fixed aspect ratio of $h : l = 1 : 10$ (width to length) is loaded with a tangential force on the top in the geometrically linear rage. The internal length scale l_c^S is varied. In Fig. 9 the bending stiffness defined as the ratio of the applied force and the top displacement is shown as a function of the ratio l_c^S/h in a double logarithmic scale.

In this example a strong size effect is found. While in the range of very small and very large ratios l_c^S/h the stiffness is nearly independent of l_c^S/h the intermediate range is governed by a power law behavior.

Both examples presented above show the physical evidence of the proposed model. Furthermore, it should be possible to determine the material parameters of the standard part of the model from uniaxial experiments like the tension test or the consolidation test. In both cases the additional degrees of freedom of the micropolar theory are not activated. In a second step, the *Cosserat* parameter may be determined from experiments with inhomogeneous distributions of stresses and strains, where the rotational degrees of freedom become important. Typical examples are the shear test or the bending problem as discussed above.

6 Conclusions

In the present study a micropolar two phase model was discussed. Based on the concept of superimposed continua the extended kinematical relations were used to describe the deformation behavior of a micropolar elastic porous material. The required balance equations were formulated for the isothermal case in the sense of Truesdell's metaphysical principles.

In the framework of the theory of porous media the volume fractions were introduced as internal variables. Therefore an evolution equation for the volume fraction of the skeleton was motivated and taken into account when the *Clausius-Duhem* inequality was evaluated. Furthermore, thermodynamically consistent constitutive equations were presented. These results are valid for a model with compressible constituents and can be modified in order to fit for the so-called hybrid and incompressible model. In the latter case, the saturation pressure explicitly enters the model.

Some examples were discussed, which show the physical evidence of the proposed model. It is found that micropolarity plays an important role if the treated problems are governed by shear or bending.

References

1. C. Truesdell, Sulle basi della termomeccanica. *Rend. Lincei (8)*, 22:33–38, 158–166, 1957
2. C. Truesdell & R. A. Toupin. The classical field theories. In S. Flügge, editor, Handbuch der Physik III/1, pages 226–793. Springer-Verlag, Berlin 1960
3. R. M. Bowen, Incompressible porous media models by use of the theory of mixtures. Int. J. Engng. Sci., 18:1129–1148, 1980
4. R. M. Bowen, Compressible porous media models by use of the theory of mixtures. Int. J. Engng. Sci., 20:697–735, 1982
5. R. de Boer & W. Ehlers, Theorie der Mehrkomponentenkontinua mit Anwendung auf bodenmechanische Probleme, Teil I. Forschungsberichte aus dem Fachbereich Bauwesen 40, Universität-GH-Essen, 1986
6. W. Ehlers, Poröse Medien – Ein kontinumsmechanisches Modell auf der Basis der Mischungstheorie. Forschungsberichte aus dem Fachbereich Bauwesen 45, Universtität-GH-Essen, 1989
7. W. Ehlers, Constitutive equations for granular materials in geomechanical context. In K. Hutter, editor, Continuum mechanics in environmental sciences and geophysics, CISM Courses and Lectures No. 337, pages 313–402. Springer-Verlag, Wien, 1993
8. E. Cosserat & F. Cosserat, Théorie des corps déformable. A. Hermann et Fils, Paris, 1909

9. A. C. Eringen & C. B. Kafadar, Polar field theories. In A. C. Eringen, editor, Continuum Physics, Vol IV – Polar and nonlocal field theories, pages 1–73. Academic Press, New York, 1976
10. D. Besdo, Inelastic behaviour of plane frictionless block-systems described as Cosserat media. Arch. Mech., 37:603–619, 1985
11. B. Zastrau, Zur Berechnung orientierter Kontinua – Entwicklung einer Direktortheorie und Anwendung der Methode der Finiten Elemente. Fortschrittberichte der VDI-Zeitschriften, Reihe 4 (Bauingenieurwesen) Nr. 60, VDI-Verlag, Düsseldorf, 1981
12. R. de Borst, Simulation of strain localization: A reappraisal of the Cosserat continuum. Eng. Comp., 8:317–332, 1991
13. W. Ehlers & W. Volk, On theoretical and numerical methods in the theory of porous media based on polar and non-polar solid materials. Int. J. Solids Struct., 35:4597–4617, 1998
14. P. Steinmann, A micropolar theory of finite deformation and finite rotation multiplicative elastoplasticity. Int. J. Solids Struct., 31:1063–1084, 1994
15. S. Diebels & W. Ehlers, On basic equations of multiphase micropolar materials. Technische Mechanik, 16:77–88, 1996
16. R. de Boer, Vektor- und Tensorrechnung für Ingenieure. Springer-Verlag, Berlin, 1982
17. S. Diebels, Constitutive modelling of micropolar porous media. In J.-F. Thimus et al., editors, Poromechanics – A Tribute to Maurice A. Biot, pages 71–76. A. A. Balkema, Rotterdam, 1998
18. S. Diebels, A micropolar theory of porous media: Constitutive modelling. Transport in Porous Media, 34:193–208, 1999
19. C. Truesdell, Thermodynamics of diffusion. In C. Truesdell, editor, Rational Thermodynamics (2nd ed.), pages 219– 236. Springer-Verlag, New York, 1984
20. A. C. Eringen, Simple microfluids. Int. J. Engng. Sci., 2:205–217, 1964
21. I-S. Liu, Method of Lagrange multipliers for exploitation of the entropy principle. Arch. Rat. Mech. Anal., 46:131–148, 1972
22. I-S. Liu & I. Müller, Thermodynamics of mixture of fluids. In C. Truesdell, editor, Rational Thermodynamcis (2nd ed.), pages 264–285. Springer-Verlag, New York, 1984
23. B. D. Coleman & W. Noll, The thermodynamics of elastic materials with heat conduction and viscosity. Arch. Rat. Mech. Anal., 13:167–178, 1963
24. W. Ehlers, On thermodynamics of elasto-plastic porous media. Arch. Mech., 41:73–93, 1989
25. B. Svendsen & K. Hutter, On the thermodynamics of a mixture of isotropic materials with constraints. Int. J. Engng. Sci., 33:2021–2054, 1995
26. W. Ehlers, P. Ellsiepen, P. Blome, D. Mahnkopf, & B. Markert, Theoretische und numerische Studien zur Lösung von Rand- und Anfangswertproblemen in der Theorie Poröser Medien, Bericht aus dem Institut für Mechanik (Bauwesen) Nr. 99-II-1. Universtität Stuttgart, 1999. Abschlußbericht zum gleichnamigen DFG-Projekt
27. K. Hutter, K. Jöhnk, & B. Svendsen, On interfacial transition conditions in two phase gravity flow. ZAMP, 45:746–762, 1994
28. T. Wu, K. Hutter, & B. Svendsen, On shear flow of a saturated ice-sediment mixture with thermodynamical equilibrium pressure and momentum exchange. Proc. R. Soc. Lond., A 454:71–88, 1998
29. J. P. Boehler, Representations for isotropic and anisotropic non-polynomial tensor functions. In J. P. Boehler, editor, Applications of tensor functions in solid mechanics, CISM Courses and Lectures No. 292, pages 31–53. Springer-Verlag, Wien, 1987
30. J. C. Simo & R. L. Taylor, Penalty function formulations for incompressible nonlinear elastostatics. Comp. Methods Appl. Mech. Engng., 35:107–118, 1982
31. R. de Borst, Numerical modelling of bifurcation and localization in cohesive-frictional materials. Pageoph., 137:368–390, 1991
32. L. Šuklje, Rheological Aspects of Soil Mechanics. Wiley-Interscience, London, 1969
33. W. Ehlers & G. Eipper, Finite elastic deformations in liquid-saturated and empty porous solids. Transport in Porous Media, 34:179–191, 1998
34. W. Ehlers, Compressible and hybrid two-phase models in porous media theories. In Y. C. Angel, editor, Anisotropy and Inhomogeneity in Elasticity and Plasticity, AMD-vol. 158, pages 25–38. ASME, 1993
35. P. Ellsiepen (Hrsg.) PANDAS – Benutzer- und Referenzhandbuch, Bericht aus dem Institut für Mechanik (Bauwesen) Nr. 97-II-9. Universität Stuttgart, 1997
36. S. Diebels & W. Ehlers. Dynamic analysis of a fully saturated porous medium accounting for geometrical and material nonlinearities. Int. J. Numer. Meth. Eng., 39:81–97, 1996
37. S. Diebels, P. Ellsiepen, & W. Ehlers, A two-phase model for viscoplastic geomaterials. In D. Besdo and R. Bogacz, editors, Dynamics of Continua, pages 103–112. Shaker Verlag, Aachen, 1998
38. S. Diebels, P. Ellsiepen, & W. Ehlers, Error-controlled Runge-Kutta time integration of a viscoplastic hybrid two-phase model. Technische Mechanik, 16:19–27, 1999
39. W. Ehlers & G. Eipper, The simple tension problem at large volumetric strains computed from hyperelastic material laws. Acta Mech., accepted, 1998
40. R. S. Lakes, Experimental microelasticity of two porous solids. Int. J. Solids Struct., 22:55–63, 1986
41. R. S. Lakes, Experimental methods for study of Cosserat elastic solids and other generalized elastic continua. In H.-B. Mühlhaus, editor, Continuum Models for Materials with Microstructure, pages 1–25. John Wiley and Sons, 1995